AGU PUBLICATIONS

Geophysical Research Letters

RESEARCH LETTER

10.1002/2015GL063602

Key Points:
- Aragonite saturation state in the North Pacific Ocean was investigated
- Seasonal amplitude of aragonite saturation was 0.4–0.6 at 50 and 100 m depths
- This was associated with variations in vertical mixing and thermocline depth

Supporting Information:
- Text S1, Figures S1–S3, and Table S1

Correspondence to:
T.-W. Kim,
twkim@kiost.ac

Citation:
Kim, T.-W., G.-H. Park, D. Kim, K. Lee, R. A. Feely, and F. J. Millero (2015), Seasonal variations in the aragonite saturation state in the upper open-ocean waters of the North Pacific Ocean, *Geophys. Res. Lett.*, *42*, 4498–4506, doi:10.1002/2015GL063602.

Received 23 FEB 2015
Accepted 10 MAY 2015
Accepted article online 13 MAY 2015
Published online 2 JUN 2015

Seasonal variations in the aragonite saturation state in the upper open-ocean waters of the North Pacific Ocean

Tae-Wook Kim[1], Geun-Ha Park[2], Dongseon Kim[1], Kitack Lee[3], Richard A. Feely[4], and Frank J. Millero[5]

[1]Marine Chemistry and Geochemistry Division, Korea Institute of Ocean Science and Technology, Ansan, South Korea, [2]East Sea Research Institute, Korea Institute of Ocean Science and Technology, Uljin, South Korea, [3]School of Environmental Science and Engineering, Pohang University of Science and Technology, Pohang, South Korea, [4]NOAA Pacific Marine Environmental Laboratory, Seattle, Washington, USA, [5]Rosenstiel School of Marine and Atmospheric Science, University of Miami, Miami, Florida, USA

Abstract Seasonal variability of the aragonite saturation state (Ω_{AR}) in the upper (50 m and 100 m depths) North Pacific Ocean (NPO) was investigated using multiple linear regression (MLR). The MLR algorithm derived from a high-quality carbon data set accurately predicted the Ω_{AR} of evaluation data sets (three time series stations and P02 section) with acceptable uncertainty ($<0.1\ \Omega_{AR}$). The algorithm was combined with seasonal climatology data, and the estimated Ω_{AR} varied in the range of 0.4–0.6 in the midlatitude western NPO, with the largest variation found for the tropical eastern NPO. These marked variations were largely controlled by seasonal changes in vertical mixing and thermocline depth, both of which determine the degree of entrainment of CO_2-rich corrosive waters from deeper depths. Our MLR-based subsurface Ω_{AR} climatology is complementary to surface climatology based on pCO_2 measurements.

1. Introduction

The North Pacific Ocean (NPO) is susceptible to ocean acidification (OA, a reduction in seawater pH primarily due to air-sea exchange of fossil fuel CO_2) [*Feely et al.*, 2004, 2008; *Sutton et al.*, 2014]. The saturation state of aragonite (a metastable form of $CaCO_3$) (Ω_{AR}) has been widely used in assessing the potential risks of OA. The Ω_{AR} parameter is calculated as $[Ca^{2+}][CO_3^{2-}]/K^*_{sp}$, where K^*_{sp} represents the apparent solubility product for aragonite. A value of $\Omega_{AR} < 1$ indicates the possibility of dissolution of aragonite shell or skeleton [*Bednaršek et al.*, 2012, 2014]. It was reported that the 100% aragonite saturation ($\Omega_{AR} = 1$) occurs in the depth range 100–1000 m in the NPO, which is much shallower than in other major basins (e.g., ~2000 m in the North Atlantic Ocean) [*Feely et al.*, 2002, 2004, 2009]. In addition, *Orr et al.* [2005] showed that increasing inputs of fossil fuel CO_2 will continue to reduce the Ω_{AR} in the NPO. The resulting aragonite undersaturation may extend to the surface near the end of this century, commencing from the subarctic NPO.

In addition to the input of fossil fuel CO_2, seasonal variation in the properties of water masses and biogeochemical processes can influence the Ω_{AR} level in the upper ocean. The resulting seasonal variation in Ω_{AR} can be larger than the trend of decreasing Ω_{AR} due to OA within a few decades. Therefore, seasonal variation in Ω_{AR} needs to be taken into account when assessing the impact of OA. Recent studies support the importance of seasonal Ω_{AR} variation in upper (<300 m) layers of the NPO coastal systems, using time series data in conjunction with an empirical relation for the interaction between Ω_{AR} and other hydrographic parameters [*Juranek et al.*, 2009, 2011; *Alin et al.*, 2012]. However, the seasonal variability of Ω_{AR} for upper (subsurface) open-ocean waters of the NPO has not been fully investigated. Although the availability of published seasonal and monthly data for ocean carbonate parameters and Ω_{AR} has enabled the estimation of the contributions of key processes to variations in Ω_{AR} in the NPO, these products have been restricted to the very surface layer [*Lee et al.*, 2000a, 2006; *Yasunaka et al.*, 2013; *Takahashi et al.*, 2014]. Indeed, we are aware of only one study showing a difference in subsurface Ω_{AR} values between summer and winter in one meridional section (25°N–55°N) of the eastern NPO [*Feely et al.*, 1988]. Practical barriers preventing basin-scale studies include a lack of seasonal data at that scale, and the difficulty in deriving an empirical algorithm that is suitable for the prediction of Ω_{AR} without loss of the regionally diverse physical and biogeochemical features and the capacity to assess their effects on Ω_{AR}

[*Bostock et al.*, 2013]. To overcome these limitations, we derived regional-specific empirical algorithms using multiple linear regression (MLR) at a spatial scale sufficient to explain local seasonal variations in Ω_{AR} (equation (1)):

$$\Omega_{AR,i} = \alpha_{0,i} + \alpha_{1,i} \cdot X_{1,i} + \alpha_{2,i} \cdot X_{2,i} + \cdots + \alpha_{n,i} \cdot X_{n,i} \quad (1)$$

where the series of X and α indicate predictor variables specific to location i and their MLR coefficients. To map the seasonal variations in Ω_{AR} for the entire NPO, the derived empirical algorithms were combined with the seasonal data for predictor variables.

2. Data Used

To derive MLR-based empirical algorithms for Ω_{AR}, we used the Pacific Ocean Interior Carbon (PACIFICA; http://cdiac.ornl.gov/oceans/PACIFICA/) data set collected from 1990 to 2008 for the NPO [*Suzuki et al.*, 2013]. The Ω_{AR} was estimated from measured total alkalinity (TA) and total inorganic carbon (TIC) data using thermodynamic constants that are consistent with the calibrated global field data [*McElligott et al.*, 1998; *Wanninkhof et al.*, 1999; *Lee et al.*, 2000b; *Millero et al.*, 2002]. These include the carbonic acid dissociation constants of *Mehrbach et al.* [1973], as refitted in a difference functional form by *Dickson and Millero* [1987], and other ancillary constants as suggested by *Millero* [1995]. The accuracies of the derived algorithms were evaluated against data collected during the GO-SHIP P02 cruise (2013) [*Swift et al.*, 2014], and from the Hawaiian Oceanographic Time-series (HOT, 1989–2013) [*Dore et al.*, 2009], and two Japanese time series stations (K2 and KNOT, 1997–2008) [*Wakita et al.*, 2010, 2013]. These data were not used in deriving the algorithms but included all seasons. Seasonal data from the World Ocean Atlas (WOA) 2013 at a resolution of 1° were combined with the empirical MLR algorithms to derive the basin-scale seasonal distributions of Ω_{AR} at various depths [*Garcia et al.*, 2013]. Months of winter, spring, summer, and fall were defined as January–March, April–June, July–September, and October–December, respectively [*Garcia et al.*, 2013]. The WOA data may not capture coastal water properties in sufficient detail because the data are skewed more toward the open ocean. Therefore, the seasonal variability of Ω_{AR} presented in this study is only valid for open-ocean waters.

3. Algorithm Development

Previous studies estimating the Ω_{AR} using MLR-based empirical algorithms for the West Coast of the USA showed that the best combination of predictor variables included temperature, oxygen, and nitrate concentrations [*Juranek et al.*, 2009, 2011; *Alin et al.*, 2012]. The chosen set of predictor variables is either directly or indirectly associated with Ω_{AR}. Therefore, we also used these parameters as the initial set of predictor variables, with the minor modification that potential temperature (θ) and apparent oxygen utilization (AOU) were used instead of temperature and oxygen. Data collected for depth $<$50 m were excluded in deriving the algorithms, so as to minimize potential biases introduced by surface ocean processes, including the air-sea exchange of oxygen. The MLR algorithms were derived using data from 50 to 800 m. We chose 800 m depth because we would like to investigate seasonal variation in the 100%, 150%, and 200% aragonite saturation horizons (see Text S1 in the supporting information). The 100% aragonite saturation horizon in the NPO usually occurs in the same depth range [*Feely et al.*, 1984, 1988, 2002, 2004, 2012].

To derive region-specific MLR algorithms, we chose a grid size of 5° × 5° because previous studies successfully predicted the Ω_{AR} at comparable spatial scales [*Juranek et al.*, 2009; *Takahashi et al.*, 2014], and this grid size achieved the prediction error to accommodate the effect of fossil fuel CO_2 in a decadal scale (~0.1 Ω_{AR}) [*Feely et al.*, 2012]. The PACIFICA data set was divided accordingly, and an independent empirical Ω_{AR} algorithm was produced for each of the 146 grid cells for which PACIFICA data were available. The best set of predictor variables was determined based on the known relation between the three preselected parameters and the Ω_{AR}, because the combinations of (i) θ, nitrate and AOU, (ii) θ and AOU, and (iii) nitrate and AOU produced the best results with similar ranges in the coefficient of determination ($r^2 > 0.97$) and root-mean-square error (0.10–0.11 Ω_{AR}) as an average for all grid cells (see Table S1 in the supporting information).

In principal, temperature should be positively correlated with Ω_{AR} and the MLR coefficients for temperature should be $>$0 because an increase in temperature would cause in a thermodynamic increase in Ω_{AR}, and

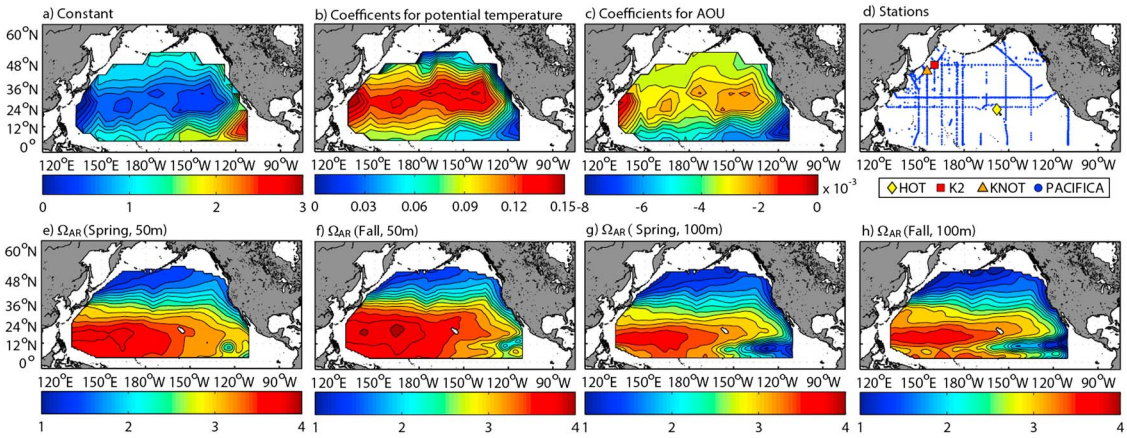

Figure 1. Distributions of multiple linear regression (MLR) coefficients for (a) constant (or intercept), (b) potential temperature, and (c) apparent oxygen utilization (AOU). (d) Station map for the PACIFICA data and time series stations (HOT, K2, and KNOT) used to derive and evaluate the MLR-based algorithms, respectively. (e–h) Distribution of Ω_{AR} at two depths (50 m and 100 m) during spring and fall.

increase water column stratification (reduced upwelling). On the other hand, AOU should be inversely correlated with the Ω_{AR} because as oxygen consumption occurs CO_2 is produced, which lowers the Ω_{AR} [*Feely et al.*, 2002, 2012; *Byrne et al.*, 2010]. This would, thus, lead to negative MLR coefficients for AOU. Only the combination of θ and AOU met these criteria. Considering all these factors, we determined that this set of parameters were optimal. All the MLR coefficients and a constant term were then interpolated for the study area (Figures 1a–1c), based on the mean latitude and longitude of data used to derive these coefficients in the defined grid cells. Residuals arising from the use of a single algorithm for the entire NPO were generally 50% greater than those for our region-specific algorithms, indicating that our approach improved prediction for studying the large-scale ocean.

The MLR algorithms based on the two additive predictor terms (θ and AOU) showed negative (measured $<$ predicted) residuals in the intermediate depths (150–500 m) and positive residuals at the other depths (50–100 m and 600–800 m). However, these depth-dependent biases (generally $<0.05\,\Omega_{AR}$) remained within the mean uncertainty of the algorithms and inevitable regardless of lower boundary depth. Inclusion of the θ-AOU interaction term reduced the bias by ~$0.03\,\Omega_{AR}$. Despite this slight improvement, we retained the MLR algorithms having only additive terms because (1) the depth-dependent bias from using only two additive predictor terms was insignificant (less than mean uncertainty) and (2) the interpolated fields of MLR coefficients appeared to be unnatural when the interaction term was included (see Figure S2 in the supporting information). Several anomalous spots were identified, and meridional and zonal gradients differed from the general distribution of physical and chemical ocean properties.

4. Algorithm Evaluations

We evaluated the predictability of the derived algorithms using a number of time series data (HOT, K2, and KNOT). The empirical algorithm underestimated Ω_{AR} for the HOT station (22.75°N, 158°W) by ~$0.07\,\Omega_{AR}$ as an average (Figure 2a), which is comparable to the uncertainty of the algorithm. The algorithms more accurately predicted Ω_{AR} for K2 and KNOT. The mean residual between the measured and predicted Ω_{AR} for both K2 and KNOT (47°N, 160°E and 44°N, 155°E, respectively) was $<0.02\ \Omega_{AR}$ (Figures 2b and 2c). Our test indicated that the derived algorithms can be used for predicting Ω_{AR} for other years in which no calibration data are available.

Seasonal bias in the empirical algorithms was also evaluated against the same time series data sets (depth range of 50–800 m). The mean differences between the measured and predicted Ω_{AR} for all seasons ranged from 0.05–0.09, 0.01–0.06, and 0.01–0.04 for the HOT, K2, and KNOT stations, respectively (Figure 2e). The differences were all within the acceptable range (i.e., $\leq \pm 0.1\ \Omega_{AR}$) and thus indicated no significant seasonal bias. The results from the analysis of the HOT station data showed that the largest difference (least prediction power) occurred during winter and spring. The errors in the wintertime were largest for

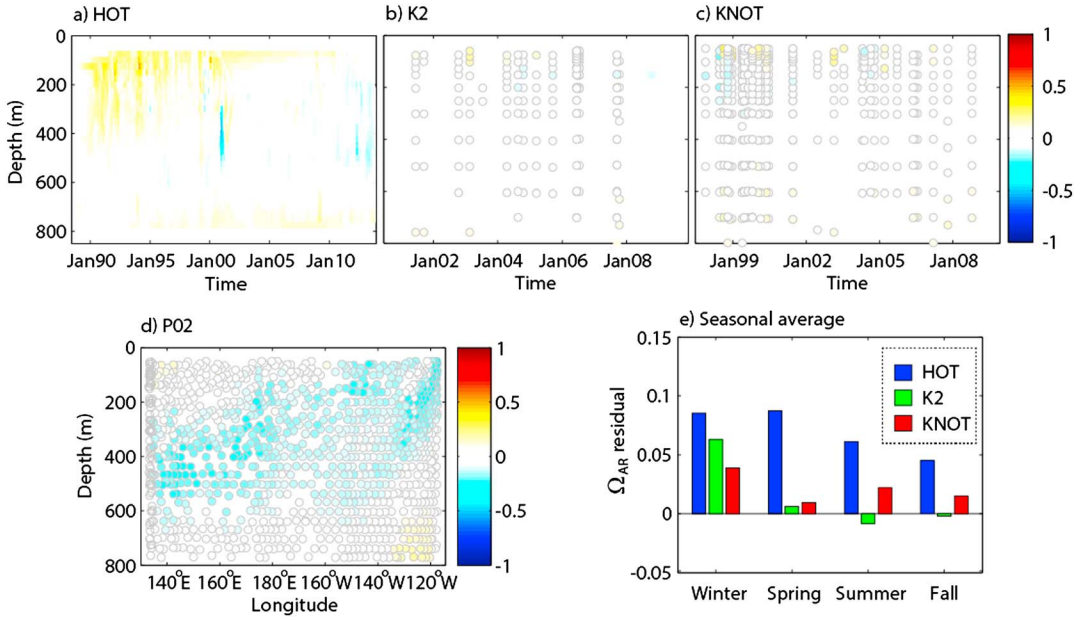

Figure 2. Residuals ($\Omega_{AR,\ MEAS} - \Omega_{AR,\ CALC}$) between the measured and predicted Ω_{AR} values at the (a) HOT, (b) K2, (c) KNOT time series stations, and (d) the P02 section occupied in 2013. The yellow and red colors indicate that our empirical algorithms underestimated Ω_{AR}, whereas the blue color indicates an overestimation. Note that Figure 2a was only contoured to avoid the data overlap caused by frequent data collection. (e) Seasonal averages of the Ω_{AR} residuals at the time series stations.

the two Japanese stations, which may be attributed to strong vertical mixing. The predictability of the derived algorithms for this season was probably reduced because of the strong influence of surface (<50 m) water, data from which were excluded when deriving the algorithms. This effect was more evident in the higher latitude Japanese stations, as revealed by the wider ranges (sixfold) of seasonal residuals than observed at the HOT station (less than twofold).

The occurrence of spatial biases was evaluated using data from the zonal P02 line (30°N) (between the east coast of Japan and the west coast of North America). Data from this zonal line are ideal for testing the predictability of algorithms for a wide range of physical and biogeochemical properties. In contrast to the results using the HOT station data, our algorithms overestimated the Ω_{AR} along this trans-Pacific line by ~0.09 Ω_{AR} as an average. The degree of overestimation did not exceed the uncertainty of the algorithms, but residual errors were locally distinct for the upper 300 m in the eastern NPO (east of 140°W) and for the intermediate depths (300–500 m) in the western NPO (west of 180°E) (Figure 2d). This error pattern appeared to be because of the inputs of fossil fuel CO_2 [*Sabine et al.*, 2002, 2004; *Feely et al.*, 2012]. However, these negative residuals were not seen in the upper layer of the western section, which also absorbed fossil fuel CO_2. The absence of the negative residuals in the western section suggests that our algorithms underestimate Ω_{AR} there.

A major weakness of this study is the incapability of the empirical algorithms to account for time-varying inputs of fossil fuel CO_2. The algorithms presented here cannot be used to account for decadal variability of the Ω_{AR} [*Juranek et al.*, 2009, 2011; *Kim et al.*, 2010]. The data collection periods used to derive independent empirical algorithms at each defined grid cell were not uniform but differed for all grids. The PACIFICA data used here covered an 18 year time span, which exceeded the period during which biases caused by the inputs of fossil fuel CO_2 remain smaller than the uncertainty of the empirical algorithms. Therefore, the data for different grids may represent different concentrations of fossil fuel CO_2, which would introduce an unavoidable error in the Ω_{AR} prediction. It is noteworthy that the effects of fossil fuel CO_2 probably disappeared when the differences among seasons were assessed because the biases were canceled out.

The input of fossil fuel CO_2 also influenced the predictability of the algorithms when there was a considerable time interval between collection of the calibration and evaluation data sets. For example, the PACIFICA

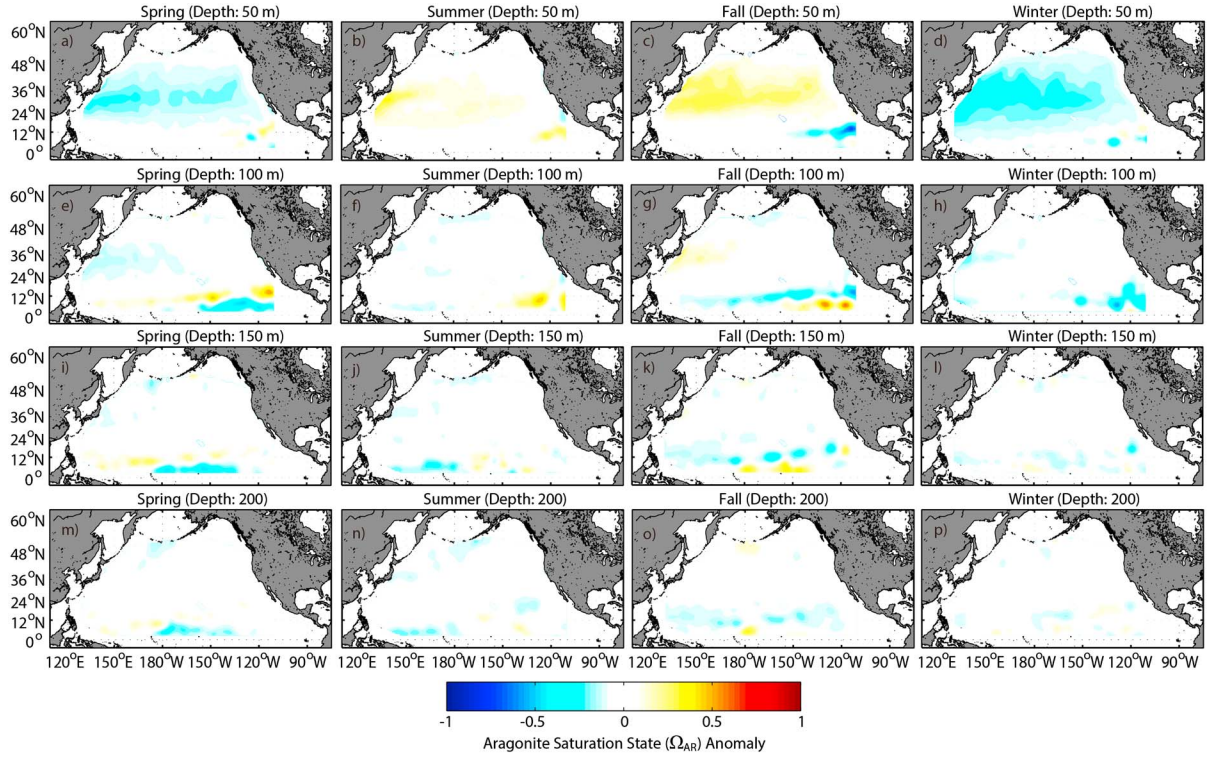

Figure 3. Seasonal Ω_{AR} anomaly during all seasons at four depths.

data near the HOT station were collected in 2006 and thus affected by a greater influence of fossil fuel CO_2 compared to the HOT station data collected during the 1990s. The decrease in Ω_{AR} by fossil fuel CO_2 would be comparable to ~0.08 Ω_{AR} from the 1990s to 2006 at the HOT station (based on a reported decreasing rate of 0.0076 Ω_{AR} per year [*Feely et al.*, 2009]), which contributed to the underestimation by our algorithm for the HOT station (Figure 2a). Similarly, for the 30°N zonal transect, the earlier collection (by 9–19 years) of calibration data relative to evaluation data resulted in overestimations by our algorithms (Figure 2d). Therefore, the evaluation errors included systematic biases arising from the input of fossil fuel CO_2, and our algorithms predicted the Ω_{AR} of the evaluation data sets better than those determined above.

5. Seasonal Variability in Ω_{AR}

The interpolated (region-specific) MLR coefficients were combined with the seasonal climatology data from the WOA 2013 (1° × 1°) to produce comparable distributions of Ω_{AR} for several depths for which seasonal variability is large. The resulting distributions largely correspond with the distribution of the Ω_{AR} in overlying open-ocean waters of the NPO [*Feely et al.*, 2004, 2012]. In the spring and summer, the value of Ω_{AR} ranged from 1.2–4.0 and 1.2–3.6 at depths of 50 m and 100 m, respectively, with the higher values being recorded in the subtropics and western tropics (Figure 1 and Figure S1 in the supporting information). The warm pool in the western tropical NPO had the highest Ω_{AR} due to thermal effect and a strong stratification (deep thermocline). These predicted features were consistent with the results reported by *Kuchinke et al.* [2014]. In contrast, the subarctic region (south of the Bering Sea and east of Okhotsk Sea) was exposed to the most corrosive open-ocean waters, and as a result the Ω_{AR} approached undersaturation near 100 m depth during the fall and winter [*Evans et al.*, 2013; *Wakita et al.*, 2013]. In addition to the trend of poleward decrease, the Ω_{AR} east of ~135°W decreased toward the west coast of North America because of the upwelling in the eastern boundary current regions [*Feely et al.*, 2008; *Gruber et al.*, 2012; *Hauri et al.*, 2013].

The westward expansion of corrosive water was clearly seen at 100 m depth along ~10°N in the eastern tropical (south of 16°N) NPO; this receives low oxygen and corrosive waters from the Central American coast, where water ventilation is sporadic and biological productivity is moderately high due to wind-induced seasonal

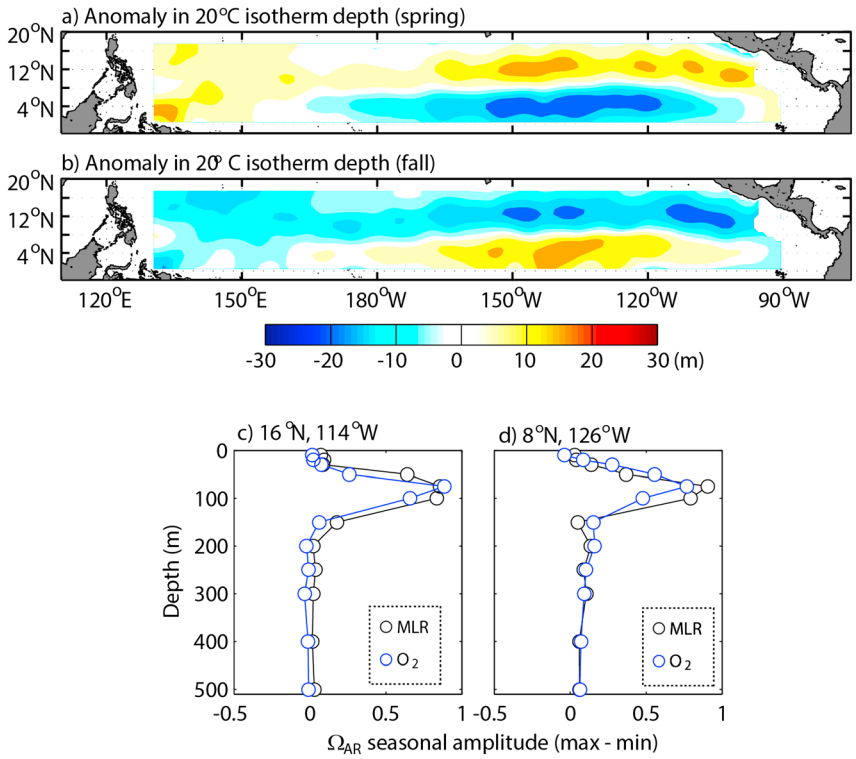

Figure 4. Anomaly in the depth of 20°C isotherm during (a) spring and (b) fall. Vertical profiles of seasonal amplitude (max − min) of Ω_{AR} for 4° × 4° areas centered at (c) 16°N, 114°W and (d) 8°N, 126°W. The black and blue symbols represent multiple linear regression (MLR)-based predictions and O_2-based estimates, respectively. The O_2-based estimates were obtained from the observed total alkalinity (TA) and total inorganic carbon (TIC) values [*Key et al.*, 2004] and the amount of change in TIC expected due to seasonal amplitude of the O_2 concentration based on the ratio of *Anderson and Sarmiento* [1994].

upwelling [*Pennington et al.*, 2006]. This feature is less discernible in the surface layer [*Takahashi et al.*, 2014], providing strong justification for our MLR-based approach despite the existing pCO_2-based surface climatology of the Ω_{AR}. The MLR-based algorithms are relatively less reliable in the surface layer because predictor variables like oxygen (or AOU) and nutrient concentrations are affected by air-sea gas exchange, N_2 fixation, and atmospheric deposition without there being corresponding change in Ω_{AR} [*Juranek et al.*, 2009, 2011; *Kim et al.*, 2011; *Evans et al.*, 2013]. Therefore, MLR algorithm-based and pCO_2-based methods can be complementary; the combination of both methods better captures seasonal and regional OA dynamics.

Seasonal variations in Ω_{AR} were clearly seen in the anomaly plots (each season versus annual mean) (Figure 3). In the subsurface (50 and 100 m depths), fall and spring showed more distinct seasonal variations. Therefore, we focused primarily on the fall and spring distributions of Ω_{AR}. Seasonal Ω_{AR} variations were largest at 50 m depth throughout most of the midlatitude region (20–40°N) (Figure 3), where the impact of temperature variation on Ω_{AR} was greatest (corresponding to the highest MLR coefficients for θ; Figure 1b). However, our algorithms could not reproduce the large seasonal variation off the West Coast of United States, probably because of the use of open-ocean climatology (WOA) for predicting seasonal Ω_{AR}. In the remaining midlatitude regions the values of Ω_{AR} were lower in spring by 0.1–0.2 Ω_{AR} than the annual mean values, whereas in fall the same regions showed positive anomalies (0.2–0.3 Ω_{AR}). These seasonal variations at 50 m depth almost disappeared at 100 m depth. Three factors can influence the observed variability at 50 m depth [*Feely et al.*, 1988]: (1) temperature-driven change in thermodynamics of carbonate system, (2) vertical mixing, and (3) biological uptake of CO_2. Under the given seasonal temperature variations (only several degree), the first factor has negligible impact on the Ω_{AR} variation [*Feely et al.*, 1988; *Takahashi et al.*, 2014]. The majority of the midlatitude NPO (except for southern boundary areas like the HOT station) typically exhibits relatively lower temperatures but higher biological productivity in spring than in fall. If the third factor was a main driver, the Ω_{AR} values in spring were higher than in fall because of higher biological

drawdown of CO_2 in spring than in fall. The intensity of vertical mixing probably dominantly controlled seasonal variability of Ω_{AR} at 50 m depth in the midlatitude NPO region. Cold water temperature in spring indicates enhanced vertical mixing, which brings corrosive water from depths to this layer, and thereby lowers Ω_{AR} values at this layer.

A contrasting vertical trend was apparent in the tropical zone (south of 20°N) where seasonal variability was enhanced at 100 m relative to shallower depths. At this depth, the spring Ω_{AR} values were greater (by 0.2–0.5) than the annual mean values (positive anomaly in spring) in the areas 10–16°N and 110–160°W (Figure 3e). This positive anomaly receded further westward. Just south of this zone (2–8°N), the sign of the Ω_{AR} anomaly was dramatically reversed during spring. The anomaly distributions were reversed during the transition from spring to fall. During fall season a narrow tongue of seasonally depressed Ω_{AR} values extended from the eastern NPO along ~12°N, while elevated Ω_{AR} values were largely confined to the eastern NPO between 2° and 8°N (Figure 3g). These dramatic shifts between seasons, and across the two tropical zonal bands at 10–16°N and 2–8°N, were consistent with the Ω_{AR} anomalies expected from the seasonality of the thermocline (Figures 4a and 4b), which can be marked by the depth of the 20°C isotherm in the eastern tropical NPO [*Kessler*, 2006]. A deeper thermocline prevents corrosive (low oxygen content and Ω_{AR}) waters from being upwelled, whereas a rise in the thermocline depth acts in the opposite direction. In this region, the seasonal variations in Ω_{AR} were consistent to those expected by the seasonal changes in oxygen concentration (Figures 4c and 4d). In addition, the most negative MLR coefficients for AOU in this region indicated the influence of corrosive waters (Figure 1c).

The seasonal thermocline variations are closely associated with wind-induced upwelling and downwelling. The contrast between wind-induced upwelling (north) and downwelling (south) is evident during the fall season between 2°N and 16°N with ~8°N as a center [*Xie and Hsieh*, 1995]. However, both of upwelling and downwelling are considerably reduced in spring, which deepens and shoals springtime thermocline in the northern and southern regions, respectively (relative to fall). The seasonal thermocline variations can be also explained by the seasonal fluctuation of North Equatorial Current/Countercurrents (NEC/NECC). The eastward velocity of NECC (centered at ~5°N) is generally least during March and April [*Hsin and Qiu*, 2012], which reduces the eastward transport of warm water and thereby results in a relatively shallower thermocline during spring. In contrast, the NEC (10–20°N) is weakest during October and November [*Kuchinke et al.*, 2014]. The influence of thermocline depth (related to wind-induced upwelling/downwelling and ocean currents) on subsurface Ω_{AR} demonstrates the importance of physical processes on the variability of Ω_{AR}.

6. Conclusions

Regionally varying MLR coefficients (calculated at grid cells) were used to predict Ω_{AR} in the NPO. In combination with climatology of θ and AOU, we established the distributions and seasonal variation in Ω_{AR} in the upper open-ocean waters. The approach used was not applicable to coastal water. The seasonal amplitude (0.4–0.6) in Ω_{AR} that we found in the subsurface layer (50–100 m) of the western midlatitude and eastern tropical NPO were larger than the changes in Ω_{AR} that have occurred over recent decades as a consequence of increased inputs of fossil fuel CO_2. In some regions, the seasonal amplitude approached ~1 Ω_{AR} (Figures 4c and 4d). Region-specific MLR algorithm can be particularly useful for studies of open-ocean areas having varying oceanographic characteristics. The method has greater predictive ability compared with a single MLR algorithm for the entire basin. In addition, the interpolation of MLR coefficients can avoid issues related to the boundaries between grid cells because the MLR coefficient changes with location. Fixed boundaries may not be adequate for studying time-dependent processes, because such boundaries are annually and seasonally dynamic, and are often difficult to determine. The direct interpolation of measured Ω_{AR} values instead of MLR coefficients can also avoid the boundary issue but cannot provide any meaningful information regarding seasonal variability.

Acknowledgments
This work was supported by Korea Institute of Ocean Science and Technology (PE99246/99201) and Basic Science Research Program (2012R1A6A3A04038883) funded by Ministry of Education and the National Research Foundation (NRF) of Korea. Partial support was provided by "Development of satellite based ocean carbon flux model for seas around Korea" funded by the Ministry of Ocean and Fisheries (MOF). Partial support for K.L. was provided by Global Research Project funded by the NRF and "Management of marine organisms causing ecological disturbance and harmful effects" funded by the MOF. R.A.F. was supported by the National Oceanic and Atmospheric Administration under the NOAA Ocean Acidification Program and the Climate Observations Division of the NOAA Climate Program. F.J.M. and R.A.F. acknowledge the financial support of the National Science Foundation and the NOAA for supporting our ocean carbon studies. Contribution number 4288 from the NOAA Pacific Marine Environmental Laboratory.

The Editor thanks two anonymous reviewers for their assistance in evaluating this paper.

References

Alin, S. R., R. A. Feely, A. G. Dickson, J. M. Hernández-Ayón, L. W. Juranek, M. D. Ohman, and R. Goericke (2012), Robust empirical relationships for estimating the carbonate system in the southern California Current System and application to CalCOFI hydrographic cruise data (2005–2011), *J. Geophys. Res.*, *117*, C05033, doi:10.1029/2011JC007511.

Anderson, L. A., and J. L. Sarmiento (1994), Redfield ratios of remineralization determined by nutrient data analysis, *Global Biogeochem. Cycles*, *8*(1), 65–80, doi:10.1029/93GB03318.

Bednaršek, N., et al. (2012), Extensive dissolution of live pteropods in the Southern Ocean, *Nat. Geosci.*, *5*(12), 881–885.
Bednaršek, N., G. A. Tarling, D. C. E. Bakker, S. Fielding, and R. A. Feely (2014), Dissolution dominating calcification process in polar pteropods close to the point of aragonite undersaturation, *PLoS One*, *9*(10), e109183, doi:10.1371/journal.pone.0109183.
Bostock, H. C., S. E. M. Fletcher, and M. J. M. Williams (2013), Estimating carbonate parameters from hydrographic data for the intermediate and deep waters of the Southern Hemisphere oceans, *Biogeosciences*, *10*(10), 6199–6213.
Byrne, R. H., S. Mecking, R. A. Feely, and X. Liu (2010), Direct observations of basin-wide acidification of the North Pacific Ocean, *Geophys. Res. Lett.*, *37*, L02601, doi:10.1029/2009GL040999.
Dickson, A. G., and F. J. Millero (1987), A comparison of the equilibrium constants for the dissociation of carbonic acid in seawater media, *Deep Sea Res. Part A*, *34*(10), 1733–1743.
Dore, J. E., R. Lukas, D. W. Sadler, M. J. Church, and D. M. Karl (2009), Physical and biogeochemical modulation of ocean acidification in the central North Pacific, *Proc. Natl. Acad. Sci. U.S.A.*, *106*(30), 12,235–12,240.
Evans, W., J. T. Mathis, P. Winsor, H. Statscewich, and T. E. Whitledge (2013), A regression modeling approach for studying carbonate system variability in the northern Gulf of Alaska, *J. Geophys. Res. Oceans*, *118*, 476–489, doi:10.1029/2012JC008246.
Feely, R. A., R. H. Byrne, P. R. Betzer, J. F. Gendron, and J. G. Acker (1984), Factors influencing the degree of saturation of the surface and intermediate waters of the North Pacific Ocean with respect to aragonite, *J. Geophys. Res.*, *89*(C6), 10,631–10,640, doi:10.1029/JC089iC06p10631.
Feely, R. A., R. H. Byrne, J. G. Acker, P. R. Betzer, C.-T. A. Chen, J. F. Gendron, and M. F. Lamb (1988), Winter-summer variations of calcite and aragonite saturation in the Northeast Pacific, *Mar. Chem.*, *25*(3), 227–241.
Feely, R. A., et al. (2002), In situ calcium carbonate dissolution in the Pacific Ocean, *Global Biogeochem. Cycles*, *16*(4), 1144, doi:10.1029/2002GB001866.
Feely, R. A., C. L. Sabine, K. Lee, W. Berelson, J. Kleypas, V. J. Fabry, and F. J. Millero (2004), Impact of anthropogenic CO_2 on the $CaCO_3$ system in the oceans, *Science*, *305*(5682), 362–366.
Feely, R. A., C. L. Sabine, J. M. Hernandez-Ayon, D. Ianson, and B. Hales (2008), Evidence for upwelling of corrosive "acidified" water onto the continental shelf, *Science*, *320*(5882), 1490–1492.
Feely, R. A., S. C. Doney, and S. R. Cooley (2009), Ocean acidification: Present conditions and future changes in a high-CO_2 world, *Oceanography*, *22*(4), 36–47.
Feely, R. A., C. L. Sabine, R. H. Byrne, F. J. Millero, A. G. Dickson, R. Wanninkhof, A. Murata, L. A. Miller, and D. Greeley (2012), Decadal changes in the aragonite and calcite saturation state of the Pacific Ocean, *Global Biogeochem. Cycles*, *26*, GB3001, doi:10.1029/2011GB004157.
Garcia, H. E., R. A. Locarnini, T. P. Boyer, J. I. Antonov, O. K. Baranova, M. M. Zweng, J. R. Reagan, and D. R. Johnson (2013), *World Ocean Atlas 2013 Volume 3: Dissolved Oxygen, Apparent Oxygen Utilization, and Oxygen Saturation. NOAA Atlas NESDIS 75*, National Oceanographic Data Center, Silver Spring, Md.
Gruber, N., C. Hauri, Z. Lachkar, D. Loher, T. L. Frölicher, and G.-K. Plattner (2012), Rapid progression of ocean acidification in the California Current System, *Science*, *337*(6091), 220–223.
Hauri, C., N. Gruber, M. Vogt, S. C. Doney, R. A. Feely, Z. Lachkar, A. Leinweber, A. M. P. McDonnell, M. Munnich, and G.-K. Plattner (2013), Spatiotemporal variability and long-term trends of ocean acidification in the California Current System, *Biogeosciences*, *10*, 193–216.
Hsin, Y. C., and B. Qiu (2012), Seasonal fluctuations of the surface North Equatorial Countercurrent (NECC) across the Pacific basin, *J. Geophys. Res.*, *117*, C06001, doi:10.1029/2011JC007794.
Juranek, L. W., R. A. Feely, W. T. Peterson, S. R. Alin, B. Hales, K. Lee, C. L. Sabine, and J. Peterson (2009), A novel method for determination of aragonite saturation state on the continental shelf of central Oregon using multi-parameter relationships with hydrographic data, *Geophys. Res. Lett.*, *36*, L24601, doi:10.1029/2009GL040778.
Juranek, L. W., R. A. Feely, D. Gilbert, H. Freeland, and L. A. Miller (2011), Real-time estimation of pH and aragonite saturation state from Argo profiling floats: Prospects for an autonomous carbon observing strategy, *Geophys. Res. Lett.*, *38*, L17603, doi:10.1029/2011GL048580.
Kessler, W. S. (2006), The circulation of the eastern tropical Pacific: A review, *Prog. Oceanogr.*, *69*(2–4), 181–217.
Key, R. M., A. Kozyr, C. L. Sabine, K. Lee, R. Wanninkhof, J. L. Bullister, R. A. Feely, F. J. Millero, C. Mordy, and T. H. Peng (2004), A global ocean carbon climatology: Results from Global Data Analysis Project (GLODAP), *Global Biogeochem. Cycles*, *18*, GB4031, doi:10.1029/2004GB002247.
Kim, T.-W., K. Lee, R. A. Feely, C. L. Sabine, C.-T. A. Chen, H. J. Jeong, and K. Y. Kim (2010), Prediction of Sea of Japan (East Sea) acidification over the past 40 years using a multiparameter regression model, *Global Biogeochem. Cycles*, *24*, GB3005, doi:10.1029/2009GB003637.
Kim, T.-W., K. Lee, R. G. Najjar, H.-D. Jeong, and H. J. Jeong (2011), Increasing N abundance in the northwestern Pacific Ocean due to atmospheric nitrogen deposition, *Science*, *334*(6055), 505–509.
Kuchinke, M., B. Tilbrook, and A. Lenton (2014), Seasonal variability of aragonite saturation state in the Western Pacific, *Mar. Chem.*, *161*, 1–13.
Lee, K., R. Wanninkhof, R. A. Feely, F. J. Millero, and T. H. Peng (2000a), Global relationships of total inorganic carbon with temperature and nitrate in surface seawater, *Global Biogeochem. Cycles*, *14*, 979–994, doi:10.1029/1998GB001087.
Lee, K., F. J. Millero, R. H. Byrne, R. A. Feely, and R. Wanninkhof (2000b), The recommended dissociation constants for carbonic acid in seawater, *Geophys. Res. Lett.*, *27*(2), 229–232, doi:10.1029/1999GL002345.
Lee, K., L. T. Tong, F. J. Millero, C. L. Sabine, A. G. Dickson, C. Goyet, G. H. Park, R. Wanninkhof, R. A. Feely, and R. M. Key (2006), Global relationships of total alkalinity with salinity and temperature in surface waters of the world's oceans, *Geophys. Res. Lett.*, *33*, L19605, doi:10.1029/2006GL027207.
McElligott, S., R. H. Byrne, K. Lee, R. Wanninkhof, F. J. Millero, and R. A. Feely (1998), Discrete water column measurements of CO_2 fugacity and pH_T in seawater: A comparison of direct measurements and thermodynamic calculations, *Mar. Chem.*, *60*(1–2), 63–73.
Mehrbach, C., C. H. Culberson, J. E. Hawley, and R. M. Pytkowicz (1973), Measurement of the apparent dissociation constants of carbonic acid in seawater at atmospheric pressure, *Limnol. Oceanogr.*, *18*, 897–907.
Millero, F. J. (1995), Thermodynamics of the carbon dioxide system in the oceans, *Geochim. Cosmochim. Acta*, *59*(4), 661–677.
Millero, F. J., D. Pierrot, K. Lee, R. Wanninkhof, R. Feely, C. L. Sabine, R. M. Key, and T. Takahashi (2002), Dissociation constants for carbonic acid determined from field measurements, *Deep Sea Res., Part I*, *49*(10), 1705–1723.
Orr, J. C., et al. (2005), Anthropogenic ocean acidification over the twenty-first century and its impact on calcifying organisms, *Nature*, *437*(7059), 681–686.
Pennington, J. T., K. L. Mahoney, V. S. Kuwahara, D. D. Kolber, R. Calienes, and F. P. Chavez (2006), Primary production in the eastern tropical Pacific: A review, *Prog. Oceanogr.*, *69*(2–4), 285–317.
Sabine, C. L., R. A. Feely, R. M. Key, J. L. Bullister, F. J. Millero, K. Lee, T. H. Peng, B. Tilbrook, T. Ono, and C. S. Wong (2002), Distribution of anthropogenic CO_2 in the Pacific Ocean, *Global Biogeochem. Cycles*, *16*(4), 1083, doi:10.1029/2001GB001639.
Sabine, C. L., et al. (2004), The oceanic sink for anthropogenic CO_2, *Science*, *305*(5682), 367–371.

Sutton, A. J., R. A. Feely, C. L. Sabine, M. J. McPhaden, T. Takahashi, F. P. Chavez, G. E. Friederich, and J. T. Mathis (2014), Natural variability and anthropogenic change in equatorial Pacific surface ocean pCO_2 and pH, *Global Biogeochem. Cycles*, *28*, 131–145, doi:10.1002/2013GB004679.

Suzuki, T., et al. (2013), *PACIFICA Data Synthesis Project, Carbon Dioxide Information Analysis Center, Oak Ridge National Laboratory*, U.S. Department of Energy, Oak Ridge, Tennessee.

Swift, J., et al. (2014), *Carbon Dioxide, Hydrographic, and Chemical Data Obtained During the R/V Melville* Cruise in the Pacific Ocean on GO-SHIP Repeat Hydrography Sections P02_2013 (21 March–1 June, 2013), Carbon Dioxide Information Analysis Center, Oak Ridge National Laboratory US Department of Energy, Oak Ridge, Tennessee.

Takahashi, T., S. C. Sutherland, D. W. Chipman, J. G. Goddard, C. Ho, T. Newberger, C. Sweeney, and D. R. Munro (2014), Climatological distributions of pH, pCO_2, total CO_2, alkalinity, and $CaCO_3$ saturation in the global surface ocean, and temporal changes at selected locations, *Mar. Chem.*, *164*, 95–125.

Wakita, M., S. Watanabe, A. Murata, M. Honda, and N. Tsurushima (2010), *Hydrographic Data Report at Station KNOT During the 1992–2008 Cruises, Carbon Dioxide Information Analysis Center*, Oak Ridge National Laboratory US Department of Energy, Oak Ridge, Tennessee.

Wakita, M., et al. (2013), Ocean acidification from 1997 to 2011 in the subarctic western North Pacific Ocean, *Biogeosciences*, *10*(12), 7817–7827.

Wanninkhof, R., E. Lewis, R. A. Feely, and F. J. Millero (1999), The optimal carbonate dissociation constants for determining surface water pCO_2 from alkalinity and total inorganic carbon, *Mar. Chem.*, *65*(3–4), 291–301.

Xie, L., and W. W. Hsieh (1995), The global distribution of wind-induced upwelling, *Fish. Oceanogr.*, *4*(1), 52–67.

Yasunaka, S., Y. Nojiri, S.-i. Nakaoka, T. Ono, H. Mukai, and N. Usui (2013), Monthly maps of sea surface dissolved inorganic carbon in the North Pacific: Basin-wide distribution and seasonal variation, *J. Geophys. Res. Oceans*, *118*, 3843–3850, doi:10.1002/jgrc.20279.